







Article

New Insights into H₂S Adsorption on Graphene and Graphene-Like Structures: A Comparative DFT Study

Azam Salmankhani ¹, Zohre Karami ² , Amin Hamed Mashhadzadeh ^{2,3,*} ,
Mohammad Reza Ganjali ^{2,4}, Vahid Vatanpour ⁵, Amin Esmaeili ⁶ , Sajjad Habibzadeh ⁷,
Mohammad Reza Saeb ² , Vanessa Fierro ⁸  and Alain Celzard ^{8,*} 

¹ Department of Mechanical Engineering, KN University of Technology, P.O. Box 196976-4499 Tehran, Iran; azamsalmankhani@gmail.com

² Center of Excellence in Electrochemistry, School of Chemistry, College of Science, University of Tehran, P.O. Box 14155-6455 Tehran, Iran; zohrekarami.2013@yahoo.com (Z.K.); ganjali@ut.ac.ir (M.R.G.); mrsaeb2008@gmail.com (M.R.S.)

³ Department of Mechanical Engineering, Azadshahr Branch, Islamic Azad University, P.O. Box 49617-89985 Azadshahr, Iran

⁴ Biosensor Research Center, Endocrinology and Metabolism Molecular-Cellular Sciences Institute, Tehran University of Medical Sciences, P.O. Box 1411713137 Tehran, Iran

⁵ Department of Applied Chemistry, Faculty of Chemistry, Kharazmi University, P.O. Box 15719-14911 Tehran, Iran; vahidvatanpour@khu.ac.ir

⁶ Department of Chemical Engineering, College of the North Atlantic—Qatar, 24449 Arab League St, P.O. Box 24449 Doha, Qatar; amin.esmaeili-khalil-saraei@polymtl.ca

⁷ Department of Chemical Engineering, Amirkabir University of Technology (Tehran Polytechnic), P.O. Box 15875-4413 Tehran, Iran; sajjad.habibzadeh@mail.mcgill.ca

⁸ Université de Lorraine, CNRS, IJL, F-88000 Epinal, France; vanessa.fierro@univ-lorraine.fr

* Correspondence: amin.hamed.m@gmail.com (A.H.M.); alain.celzard@univ-lorraine.fr (A.C.); Tel.: +98-911-376-5114 (A.H.M.); +33-372-749-614 (A.C.)

Received: 18 September 2020; Accepted: 5 November 2020; Published: 9 November 2020



Abstract: The efficient removal of pollutants from different environments has been one of the great challenges for scientists in recent years. However, the understanding of the mechanisms underlying this phenomenon is still the subject of passionate debates, mainly due to the lack of experimental tools capable of detecting events at the atomic scale. Herein, a comparative theoretical study was carried out to capture the adsorption of H₂S on metal oxide surfaces such as zinc oxide (ZnO) and beryllium oxide (BeO), as well as graphene and Ni-decorated graphene. A simulation based on density-functional theory (DFT) was carried out by adopting General Gradient Approximation (GGA) under the Perdew–Burke–Ernzerhof (PBE) function. The calculations quantified H₂S adsorption on the considered metal oxide sheets as well as on the non-decorated graphene having a physical nature. In contrast, H₂S adsorbed on Ni-decorated graphene sheet gave an adsorption energy of −1.64 eV due to the interaction of S and Ni atoms through the formation of a covalent bond, proof of chemisorption. It seems that the graphene sheet decorated with Ni atoms is a more suitable adsorbent for H₂S molecules than BeO, ZnO, or non-decorated graphene, providing a theoretical basis for future studies.

Keywords: H₂S adsorption; metal oxide; graphene-like structures; Ni-decorated graphene; DFT

1. Introduction

H₂S is one of the air pollutants released during various processes such as petroleum refinery, natural gas and biogas processing, coking plants, wastewater treatment units, etc. [1,2]. This highly

toxic compound has raised global concerns in recent decades due to its harmful effects on the environment as well as on human health [3,4]. If inhaled, even at low concentrations, H₂S can seriously affect the nervous system, causes a feeling of weakness, coughing, and runny nose. Moreover, at higher concentrations, the consequences would be even worse, which could lead to visceral injury, coma, acidosis, and death [5,6]. In industrial processes, H₂S can cause corrosion of process equipment, contaminate pipelines, and consequently, affect product quality [7]. Moreover, excess H₂S in the environment and atmosphere can lead to acid rains and cause serious damage to crops and infrastructure [8,9].

Considering all the above-mentioned problems, the detection and adsorption of H₂S have recently been the subject of many theoretical and experimental research studies [10–12]. In this respect, different materials such as metal surfaces [13,14], ionic liquids [11], zeolites [15], and activated carbons [16,17] have been examined as potential H₂S adsorbents. In addition, the use of low-dimensional nanostructures including carbon nanotubes [18,19], fullerenes [20], pristine graphene [21], metal oxides [22,23], decorated graphene [24–26], and doped graphene [27,28] for the adsorption of gas molecules has opened up a new window on this topic due to the outstanding properties of these structures.

Since the introduction of graphene to the world in the 1990s, this 2D structure has been used in various applications, particularly in gas sensing applications. Graphene, as a *sp*²-hybridized monolayer of carbon atoms forming a hexagonal honeycomb lattice, provides great sensing properties due to its high specific surface area, good electron mobility, and excellent electronic conductivity [29,30]. However, several studies have reported a weak physisorption interaction between pristine graphene and common gas molecules [31,32]. Therefore, doping or decorating graphene with different elements has been recognized as solutions to the poor electronic properties of pristine graphene, and to create stronger interactions between graphene and gas molecules [33]. Many previous research works have been devoted to this topic, mainly based on the density-functional theory (DFT) approach. Namely, Mn-doped graphene was modeled using DFT by Jia et al. [7], who showed a significant improvement in adsorption energy and charge density, as well as the higher adsorption capacity of Mn-doped graphene toward H₂S compared to pristine graphene. In another DFT-based research, Khodadadi [28] reported that decorating graphene with different transition metals could significantly improve its H₂S sensing capability. The same kind of result was also observed in the case of graphene nanosheets doped with Fe [27,28] and Ag [34], as these metals considerably improve their adsorption properties with respect to pristine graphene by Lewis acid–base interactions.

The resulting charge transfer between the adsorbent and the adsorbate therefore changes the resistivity of the material, so that a chemiresistive graphene-based sensor system can be imagined. However, the sensitivity of the device would be too low if pristine graphene were used, due to the too weak and long-range interaction of this kind of surface with most gases at room temperature. Doping graphene with metals thus appears to be a very efficient way to adjust its adsorption properties, and hence, its ability to detect and quantify gaseous molecules by changing its conductive properties. In particular, the advantage of such a method is that the adsorption of metallic nanoparticles on graphene does not deteriorate its carrier mobility [35].

Thus, whereas too weak adsorbate–adsorbent interactions are detrimental to the sensitivity of the sensor, especially at room temperature, it can be expected that the recoverability of the sensor, i.e., its ability to release the adsorbed gas within a reasonable time and at a reasonable temperature, would be poor in the case of too strong interactions. An optimum should therefore exist between too low and too high adsorption energy, and the well-known affinity of Ni for S, although not as high as that of Ag or Pt, should be a good compromise for such an application. Moreover, Ni is one of the transition metals that has been widely used to decorate various materials and improve their adsorption properties. For instance, Gaboardi et al. [36] reported that the hydrogen adsorption capacity of graphene increased by 51% after being decorated by Ni. Therefore, Ni appears to be effective as an element for decorating graphene to improve its adsorption properties towards different substances, especially H₂S.

The remarkable properties of graphene have motivated researchers to focus on the adsorption of other types of monolayer structures such as metal oxide surfaces, including but not limited to zinc oxide (ZnO) [37,38], beryllium oxide (BeO), manganese oxide (MnO) [38], vanadium pentoxide (V_2O_5) [23], or sulfide-based and nitride-based surfaces such as molybdenum disulfide (MoS_2) [39], aluminum nitride (AlN), boron nitride (BN), and gallium nitride (GaN) [40]. Namely, the acetone adsorption properties of BeO, MgO, and ZnO surfaces were investigated in a DFT study by Mo et al. [38]. They reported satisfactory adsorption energies of all these surfaces interacting with acetone [38]. In the research by Ganji et al. [40], DFT calculations were performed to evaluate the adsorption of H_2S on graphene-like structures of aluminum nitride (AlN) and gallium nitride (GaN), and reported adsorption energies of -0.30 and -0.33 eV for AlN and GaN sheets, respectively. Based on the results, the GaN sheet with a higher adsorption energy was also identified as a relevant H_2S sensing material. Mashhadzadeh et al. [37] used graphene-like ZnO sheets and ZnO nanotubes to adsorb heavy metal atoms, including Ni^{2+} , Cu^{2+} , Ag^+ , and Cd^{2+} , using DFT calculations. Their results demonstrated that the strongest adsorption occurs between Ni^{2+} and ZnO nanotubes or sheets, compared to the other heavy metals studied. The doping of ZnO monolayers with Pd, Au, Fe, and Co was simulated by Zhang et al. [41] and, according to DFT calculations, a higher adsorption capacity of H_2S was reported for doped nanosheets compared to non-doped ones.

Given the importance of evaluating adsorption of hazardous gases on graphene-like surfaces, to the best of our knowledge, no research work has been conducted to date to provide comparison between the H_2S adsorption properties of ZnO and BeO surfaces with pristine and decorated graphene sheets. The main objective of the present study was to investigate the adsorption properties of ZnO, BeO, and pristine graphene sheets interacting with H_2S and to provide comprehensive comparisons between these results and those obtained for a Ni-decorated graphene surface. To achieve this goal, all the nanostructures mentioned were designed and geometrically optimized using DFT. Adsorption energies as well as the density of states (DOS) and partial density of states (PDOS) calculations were also generated to capture the behavior and intensity of H_2S adsorption properties of these typical surfaces. Finally, the results obtained were discussed and compared to be considered in the future development of the corresponding H_2S gas sensors. It must be clearly understood that this work is intended to be confronted with future experimental aspects, particularly in terms of feasibility and performance (efficiency of the adsorption/desorption process and problems of saturation and contamination of the layer) once such a sensor will have been designed. These considerations, therefore, go well beyond the primary objective of this article.

2. Computational Method

A classical simulation algorithm was used in this study. In the first step, the adsorption structures of H_2S molecules on BeO, ZnO, pristine graphene, and Ni-decorated graphene were modeled and geometrically optimized by DFT calculations using the “Spanish Initiative for Electronic Simulations with Thousands of Atoms (SIESTA)” code [42,43]. In order to study the electronic properties and correlation effects, we adopted the General Gradient Approximation. There is evidence that conventional DFT methods fail to precisely address the van der Waals (vdW) forces and cannot capture the dispersion interactions, despite their crucial role in weakly interacting systems [44]. Therefore, the standard DFT in the GGA approximation has been complemented by an ab initio vdW tactic offered by Grimme, known as the vdW-DFT method. It allows the incorporation of dispersive vdW interactions into the DFT. We also used split-valence double- ξ basis sets of the localized numerical atomic orbitals throughout the modeling process including polarization functions (DZPs). The energy shift was set to 50 meV and the split norm was 0.25. Furthermore, a $5 \times 5 \times 1$ Monkhorst–Pack grid was used for the k-point sampling of the Brillouin zone, while the atomic locations were relaxed until the residual forces on the atoms were below 0.02 eV/Å [43,45]. Moreover, to investigate the charge density, the mesh cutoff was set to 120 Ry applying Basis Set Superposition Error (BSSE) corrections by adding ghost atoms at all stages, which allowed us to calculate the isolated adsorbent. The use

of BSSE corrections is necessary for these kinds of calculations in order to provide accurate energies when the atoms of the system interact [46]. A periodic boundary condition was imposed on graphene and graphene-like surfaces such that the vacuum height was chosen to be equal to 20 Å. This value could eliminate slab–slab interactions. The selected supercell contained 50 atoms [47]. The systems comprising adsorbents and adsorbates were initially modeled in different possible configurations and were then allowed to relax throughout the complete optimization process. According to the BSSE corrections, the adsorption energies of the H₂S molecule interacting with the surfaces of BeO, ZnO, pristine graphene, and Ni-decorated graphene were calculated using the following equation:

$$E_{int}^{BSSE} = E(surf/H_2S) - E(surf_{ghost}/H_2S) - E(surf/H_2S_{ghost}) \quad (1)$$

where E_{int}^{BSSE} represents the interaction energy and $E(surf/H_2S)$ stands for the total energy of the nanosheet surface (*surf*) interacting with the H₂S molecule. The “ghost” in $E(surf_{ghost}/H_2S)$ and $E(surf/H_2S_{ghost})$ terms corresponds to the counterpoise corrections that use “ghost” atoms. In other words, these terms correspond to additional basis wave functions centered at the position of the H₂S molecule or the nanosheet surface (pure graphene, ZnO, BeO, or Ni-decorated graphene), but without any atomic potential. Therefore, a negative value of E_{int}^{BSSE} reflects an energetically stable adsorption configuration. Since all the calculations in this work were made at the constant temperature of 0 K, whereas in experimental work, temperature must be considered as an effective factor, it is not reasonable to compare these theoretical results with the experiments. The latter are therefore not provided here.

3. Results and Discussion

3.1. Geometrical Design and Optimization

According to the optimized H₂S structure, the H-S bond length and H-S-H bond angle were obtained as 1.360 Å and 91.68°, respectively. The values obtained are in close agreement with those reported in other studies [7,14,22]. A similar process was performed for the graphene-like ZnO and BeO structures, and the optimized structures are presented in Figure 1. The Be-O and Zn-O bond lengths were 1.57 and 1.87 Å, respectively, which is close to the values reported in previous DFT-based studies [48–53].

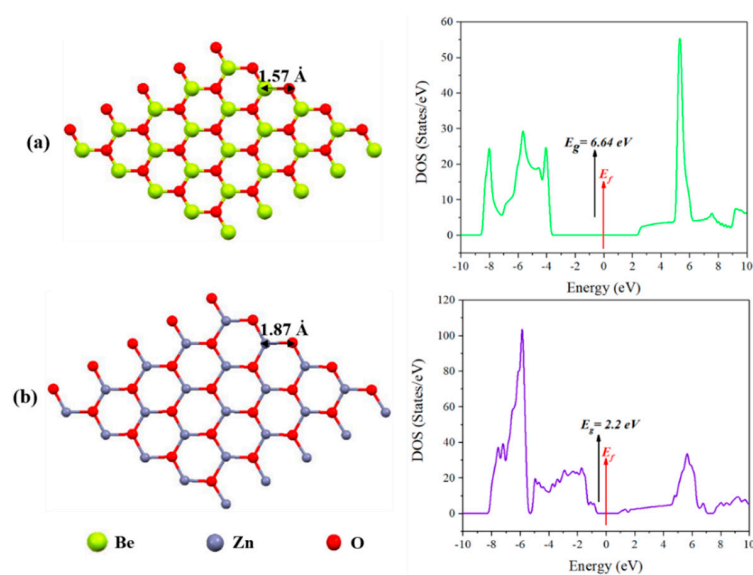


Figure 1. Optimized structures and the corresponding density of states (DOS) plots for: (a) BeO and (b) ZnO nanosheets (the Fermi level is set to zero).

In addition, Figure 1 shows the DOS diagrams of the two nanostructures. The DOS illustrates the electronic properties of the structures through the bandgap energy (E_g), which takes into account the energy difference between the highest occupied molecular orbital (HOMO) and the lowest unoccupied molecular orbital (LUMO). E_g is the minimum energy required to excite electrons from the valence band to the conduction band, so that a lower E_g means a higher electrical conductivity and a higher adsorption potential of the structure. As shown in Figure 1, the bandgap energy of the ZnO surface is equal to 2.2 eV, which is much lower than that of the BeO surface, 6.64 eV. The same kind of result has been provided by previous research regarding the bandgap of ZnO [54,55] and BeO [56,57] nanosheets, demonstrating a close agreement with our own results. Thus, ZnO sheets are more conductive than BeO sheet and hence, should exhibit higher adsorption potential when interacting with H₂S.

In the next step, we brought the H₂S molecule closer to the surface of the studied sheets in various situations. Figure 2 shows 10 different configurations as the scenarios reflecting the adsorption behavior of H₂S with H or S atoms on the hexagonal rings of the ZnO or BeO sheets. These configurations are only initial possibilities, and the position of H₂S on the surface varies during the optimization process until the molecule chooses the one that releases the most energy. These 10 initial configurations are thus sufficient to find the optimized structure. Configurations called H correspond to the sites on which the H₂S molecule approaches the surface by one of its H atoms, whereas configurations called S correspond to the sites where H₂S is brought close to the surface by its S atom. It should also be noted that in all configurations, H₂S molecules are parallel to the metal oxide surfaces. During the optimization process, the molecules rotate and select their most stable situation with the lowest equilibrium distance as well as the highest adsorption energy. The adsorption energies of H₂S at different sites of the ZnO and BeO sheets are also given in Table 1. As seen, the maximum energy released to achieve the most stable H₂S configurations is on the H2 site of BeO and the H1 site of ZnO sheets with adsorption energies of -0.144 and -0.376 eV, respectively.

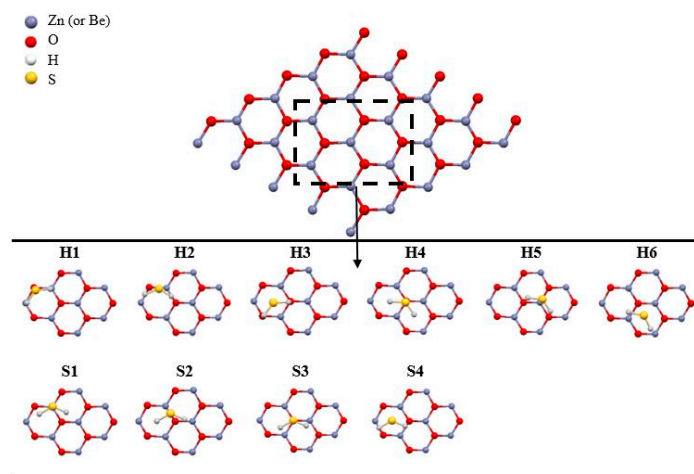


Figure 2. Schematic view of H₂S interacting with ZnO (or BeO) nanosheet in ten various adsorption configurations.

3.2. Adsorption of H₂S on Graphene-Like Metal Oxide Surfaces

As shown in Table 1, H₂S was adsorbed at all ten adsorption sites on the BeO surface with consistently negative adsorption energies, the strongest adsorption occurring at the H2 site with a value of -0.144 eV. This same site resulted in a positive adsorption energy for H₂S on graphene-like ZnO, unlike the nine other sites.

Side views of H₂S adsorption on BeO and ZnO nanosheets in the most stable configurations are displayed in Figure 3a. This figure indicates a weak interaction of the hydrogen atom of the H₂S molecule with the oxygen of the BeO surface at an equilibrium distance of 2.709 Å. Furthermore, the corresponding adsorption energy of the H1 site is -0.376 eV with the equilibrium distance of 2.820 Å

between the sulfur atom of H₂S and the zinc atom of the ZnO sheet. The DOS plot of the H₂S/BeO complex at the H2 site is displayed in Figure 3b, and it shows a reduction in the E_g from 6.64 eV for BeO alone to 5.65 eV after adsorption of H₂S. In addition, as clearly seen in Figure 3b, the DOS plot reveals that the bandgap energy is decreased from 2.2 eV for ZnO alone to 2.1 eV after adsorption of H₂S on the H1 site. Such a small difference in bandgap shows that the H₂S adsorption does not have a significant effect on the electrical properties of the ZnO nanosheet [58]. The results obtained by calculating the adsorption energy and the DOS confirm a physisorption interaction between H₂S and BeO as well as ZnO sheets, while the highest energy of adsorption of H₂S on the ZnO surface (−0.376 eV) is about three times higher than that of the same molecule on BeO (−0.144 eV).

Table 1. Calculated adsorption energies of H₂S on ZnO and BeO nanosheets at the different adsorption sites shown in Figure 2.

Adsorption Site	Adsorption Energy (eV)	
	on BeO Nanosheet	on ZnO Nanosheet
H1	−0.096	−0.376
H2	−0.144	0.011
H3	−0.114	−0.199
H4	−0.101	−0.201
H5	−0.110	−0.239
H6	−0.134	−0.236
S1	−0.127	−0.217
S2	−0.141	−0.041
S3	−0.124	−0.192
S4	−0.112	−0.359

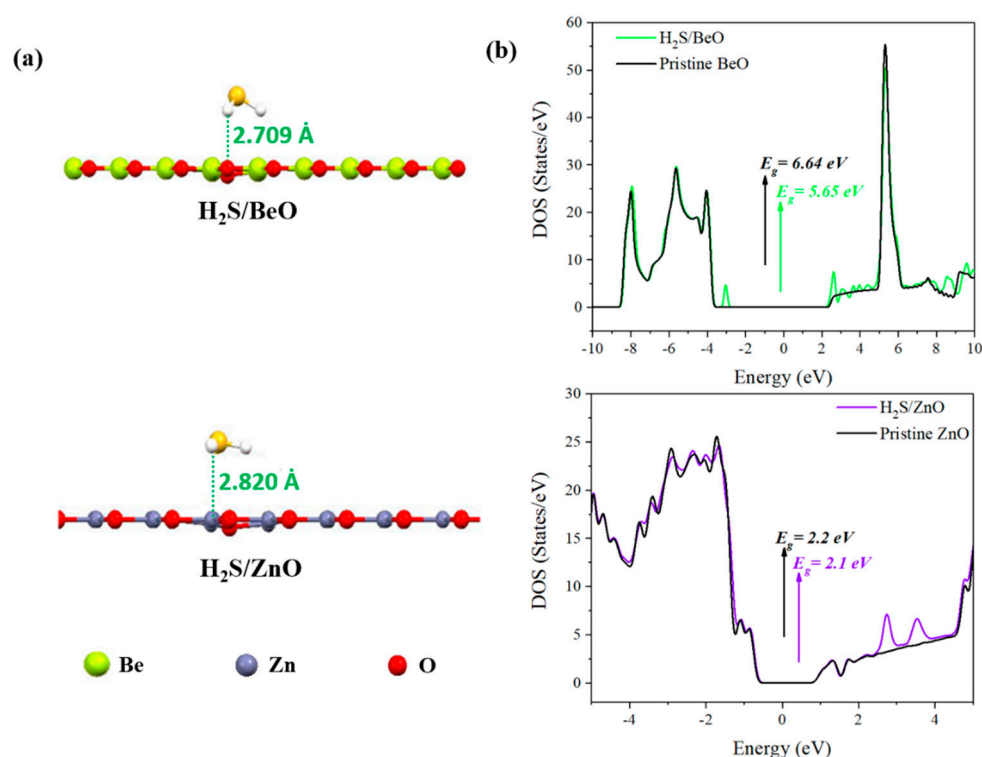


Figure 3. (a) Side views of the optimized structures and geometrical parameters of the adsorption of the H₂S molecule on the surface of BeO and ZnO nanosheets at sites H2 and H1, respectively; (b) DOS calculated for BeO and ZnO nanosheets before and after adsorption of the H₂S molecule at sites H2 and H1, respectively (the Fermi level is set to zero).

The general conclusion of the results discussed in this section is that neither BeO nor ZnO seem to be appropriate materials for H₂S gas sensors, either because of a too weak interaction between H₂S and the surface or because of a too low impact on the electrical resistance of the device. Since the synthesis of such kinds of nanosheets is also an expensive and time-consuming process, one may need to find other alternatives from more available and less expensive materials such as graphene while improving the sensing properties of graphene. Decorating the latter with various metals such as Ni could be an appropriate solution.

3.3. Adsorption of H₂S on Pristine and Ni-Decorated Graphene Nanosheets

At this stage, first, we optimized the geometrical parameters of pristine graphene based on the DFT calculation. From the observed results, we found that the length of the C-C bond of graphene in the optimized situation is about 1.42 Å, which corresponds best to the previous DFT calculations [59–61] and is also identical to the well-known length of the C-C bond in the graphite structure [62].

The adsorption of the H₂S molecule on pristine graphene was studied by DFT calculation to compare it with the result of Ni-decorated graphene sheet. Figure 4 shows seven different configurations for the adsorption of the H₂S molecule on graphene sheet. We should also mention that for all configurations, H₂S molecules are parallel to the surface of pristine graphene. Moreover, the calculated adsorption energy of H₂S at seven adsorbed sites are listed in Table 2 in order to select the most stable adsorption configuration for the H₂S molecule. As it is obvious from Table 2, H4 is the most stable site with the corresponding minimum released energy of −0.119 eV. As can be seen in the DOS graph presented in Figure 5a, the Dirac point located at the Fermi level and the bandgap energy of pristine graphene is zero. The side view of the most stable adsorption structure (H4) of the H₂S molecule on the pristine graphene surface and the corresponding DOS plot are presented in Figure 5b. As shown in this figure, 0.011e was transferred from H₂S to the graphene and the equilibrium distance between them after adsorption was 3.564 Å. The charge transfer from H₂S to the graphene increased its conductivity, which is also observable as the dispersion that occurred in the DOS plot of graphene after H₂S adsorption (see Figure 5b). Similar results were obtained experimentally by Fattah and Khatami, who showed that the electron transfer from H₂S to graphene during the adsorption process is due to the polarity of H₂S [34]. It should also be noted that the adsorption energy of the graphene/H₂S complex (−0.119 eV) is of the same order of magnitude as that reported elsewhere: −0.15 eV [27] by Cortés-Arriagada et al. using the Perdew–Burke–Ernzerhof (PBE) functional as used in this work, and −0.1 eV in the experimental study presented by Ovsianytzkyi et al. [34]. However, there are also different results in this respect, so that the results for the highest adsorption energy of the graphene/H₂S complex presented by Ganji et al. (0.02 and −0.04 eV with and without BSSE) were different from those of other studies using Perdew–Burke–Ernzerhof (PBE) and Ceperly–Alder (CA) [26]. As for the C-S distance, a value of about 3.6 Å had indeed been calculated in [27,28]. It should be stressed that the eV values depend on the methodology and assumptions involved in the development of the model and the software used. Comparing the highest adsorption energy obtained for the H₂S/pristine graphene complex (−0.119 eV) and the highest adsorption energies already calculated for the H₂S/BeO (−0.144 eV) and H₂S/ZnO (−0.376 eV) complexes, it can be concluded that metal oxide surfaces seem to be more effective as H₂S sensing materials than pristine graphene. Furthermore, the larger equilibrium distance of H₂S adsorption on pristine graphene (3.564 Å) compared to the distances previously observed for H₂S/BeO (2.709 Å) and H₂S/ZnO (2.820 Å) can be seen as more evidence. Overall, it seems that pristine graphene fails to give a sensor of H₂S at room temperature, which is why decorating graphene with a Ni atom was practiced to improve its adsorption properties. Especially, the shift from physisorption to chemisorption is necessary for adsorbent–adsorbate interactions to occur and to be maintained at room temperature.

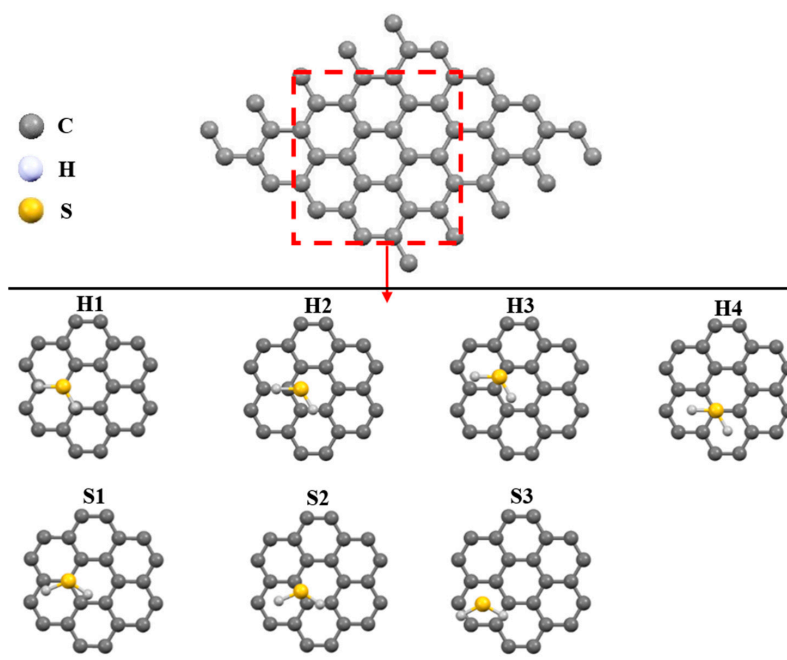


Figure 4. Schematic view of H₂S interacting with graphene sheet in seven adsorption configurations.

Table 2. Calculated adsorption energies of H₂S on pristine graphene at the different adsorbed sites shown in Figure 4.

Adsorption Site	Adsorption Energy (eV)
H1	-0.113
H2	-0.112
H3	-0.118
H4	-0.119
S1	-0.117
S2	-0.114
S3	-0.116

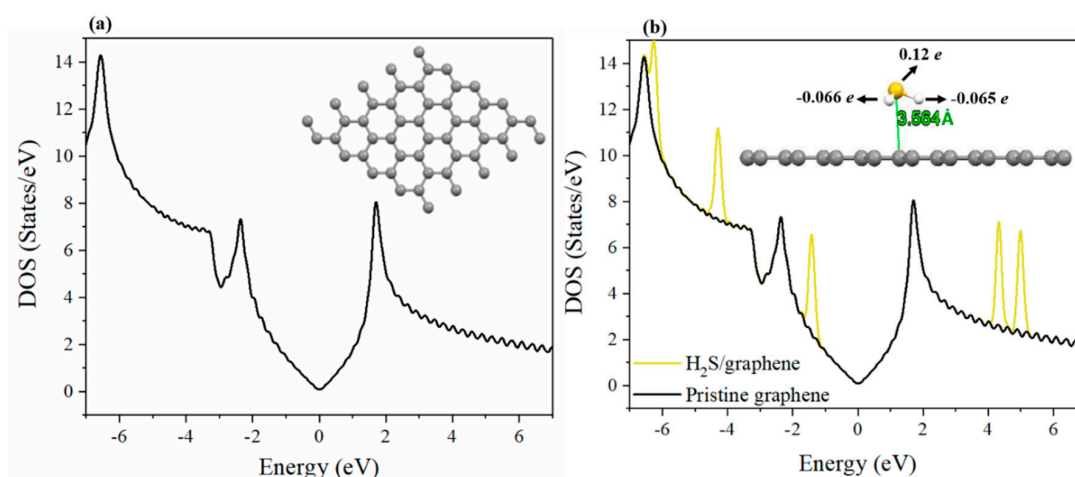


Figure 5. DOS plots for pristine graphene sheet: (a) before and (b) after adsorption of the H₂S molecule at site H4 (the Fermi level is set to zero).

As mentioned above, the H₂S molecule adsorbs on the pristine graphene by weak physical interaction. Decorating the graphene surface with Ni atoms might improve the affinity of H₂S molecules for the surface through specific interactions with Ni atoms. In this regard, three different

sites were considered for decorating the graphene surface with a Ni atom, called top (i.e., at the top of a carbon atom), hexagonal (i.e., in the hexagonal well formed by an aromatic ring), and bond (i.e., between two nearest neighboring C atoms), as illustrated in Figure 6. According to the literature, the most stable configuration of Ni-decorated graphene can be obtained by adsorption of the Ni atom on the hexagonal site of pristine graphene [63]. For this reason, this configuration was selected in the present work, and the DOS plot of the Ni-decorated structure on the hexagonal site of pristine graphene is also presented in Figure 7a. Nickel substitution in the graphene sheet has not been considered because such a configuration is very unlikely due to the considerable differences in electronic properties between the nickel and carbon elements and their differences in size.

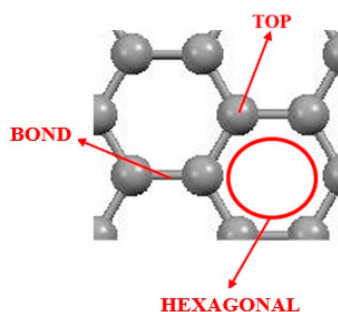


Figure 6. Top, bond, and hexagonal adsorption sites of Ni on the graphene sheet surface.

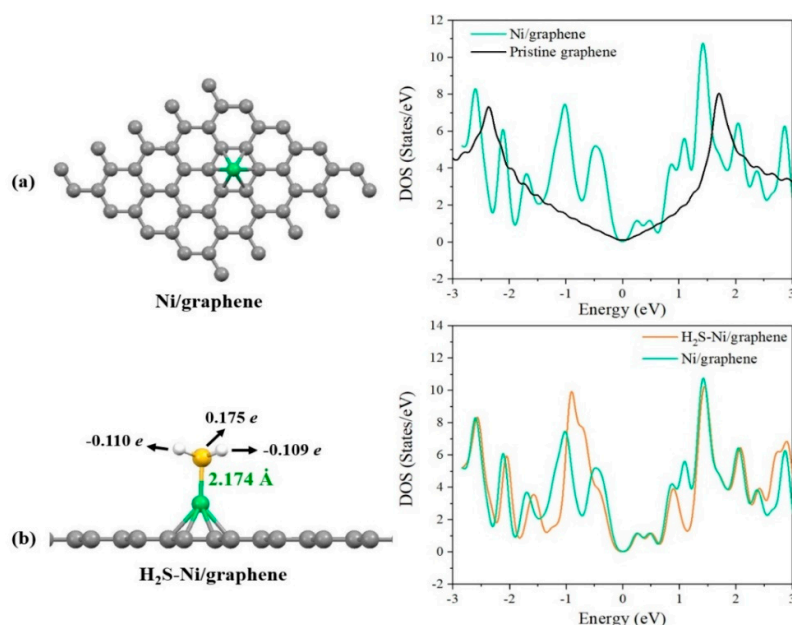


Figure 7. (a) Optimized structures of Ni-decorated graphene on the hexagonal site and corresponding DOS plot; (b) side view of the optimized structure and geometrical parameters and DOS plot calculated after adsorption of the H₂S molecule on the surface of Ni-decorated graphene (the Fermi level is set to zero).

Figure 7a shows that the DOS plot has been compressed around the Fermi level relative to the DOS plot of pristine graphene, demonstrating the formation of chemical bonds between Ni and carbon atoms of the surface. Moreover, Figure 7b displays an optimized structure and charge transfer of the H₂S molecule adsorbed on the surface of the Ni-decorated graphene complex. This figure shows that H₂S has been adsorbed on the Ni atom of the Ni-decorated graphene. As seen in Figure 7b, the Mulliken population analysis indicates that a 0.044e charge (i.e., 0.175e–0.11e–0.109e) was transferred from the H₂S molecule to the Ni/graphene complex. In other words, 0.044 electrons per H₂S molecule

is introduced into the Ni-doped graphene, which is almost four times higher than what we had already calculated for the H₂S/graphene complex (0.011e), thus corresponding to a decrease in the electrical resistance measured as a sensor response. In this configuration, the calculated adsorption energy of the H₂S molecule on the Ni-decorated graphene revealed a released energy of -1.645 eV (against -1.19 eV for Fe-doped graphene [27]). The adsorption strength is thus increased by almost 1300% compared to that of pristine graphene, which confirms the formation of a covalent bond in the H₂S/Ni-decorated graphene structure, i.e., it corresponds to a chemisorption process. Compared to the results obtained earlier in this study, the Ni-S bond length is much shorter than the equilibrium distance between H₂S and other surfaces, in good agreement with the higher adsorption energy for the Ni-decorated surface.

In the research conducted by Ganji et al. [26,40], the adsorption energies of the H₂S molecule on Al-, Ga-, and Pt-decorated graphene are -0.13 , -0.09 , and -6.37 eV, respectively. Comparison of the results of this paper with those of previous studies shows that the Ni-decorated graphene can give appropriate results in terms of absorption of the H₂S molecule. Indeed, the adsorption energy is much higher than on Al and Ga, thus allowing a good interaction with the surface (chemisorption) at room temperature, but not as high as with Pt, thus allowing a good recoverability of the sensor.

The partial density of state (PDOS) for the most stable structures of the BeO and ZnO nanosheets, as well as those of pristine and Ni-decorated graphene, were also calculated and the corresponding plots are shown in Figure 8a–d to illustrate the orbital contribution and the change in electronic structure of these surfaces after H₂S adsorption. Figure 8a demonstrates a quite weak interaction between the 2p orbital of oxygen and the 1s orbital of hydrogen, which confirms the physisorption process of H₂S molecule on the BeO surface. Likewise, in the case of H₂S molecule adsorption on the ZnO surface, a weak interaction is obvious in Figure 8b. Figure 8c,d illustrate the orbital hybridization of H₂S with pristine and Ni-decorated graphene surfaces, respectively. Figure 8c,d can be compared since there is no significant overlap between the 2p orbital of carbon and the 3p orbital of sulfur, while a strong hybridization of the Ni 3d and S 3p orbitals (especially in the range 1–4 eV; see the inset in Figure 8d) can be observed. Therefore, the strongest chemical adsorption of H₂S, which occurred on Ni-decorated graphene, might be attributed to the hybridization of the orbitals with the very good overlap that can be seen in Figure 8d [64].

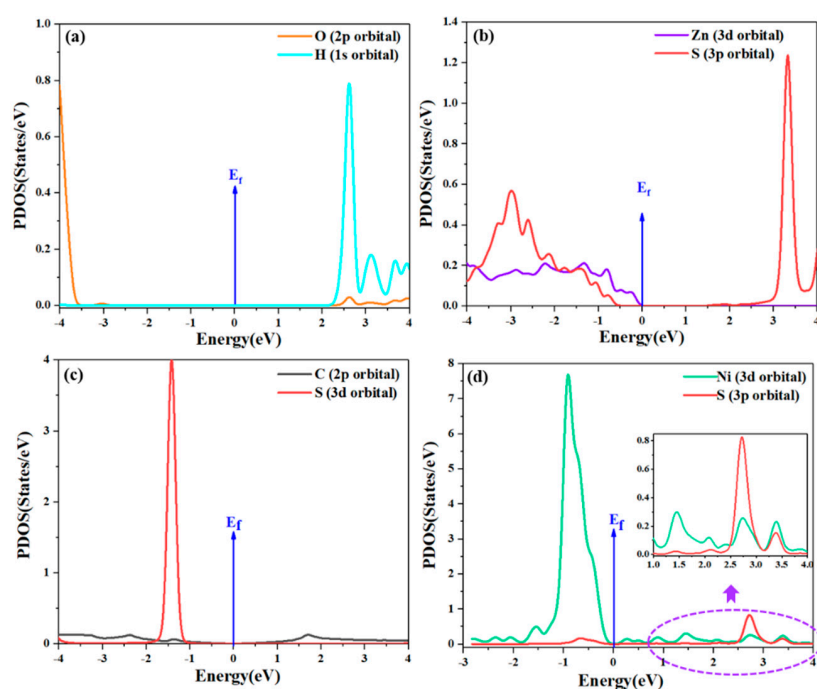


Figure 8. Partial density of states (PDOS) plots of H₂S adsorption on: (a) BeO, (b) ZnO, (c) pristine graphene, and (d) Ni-decorated graphene sheets.

4. Conclusions

In this work, the adsorption properties of graphene-like metal oxide surfaces such as BeO and ZnO with respect to the H₂S molecule were evaluated by DFT calculations. These properties were compared to the adsorption properties of pristine and Ni-decorated graphene sheets. The results showed that the H₂S molecule physically adsorbs on BeO and ZnO surfaces with adsorption energies of -0.144 and -0.376 eV, respectively. Similarly, in the case of pristine graphene, the H₂S molecule physisorbs on the surface, releasing an energy of -0.119 eV. In contrast, the DFT calculations demonstrated a chemisorption process of the H₂S molecule on the Ni-decorated graphene sheet with an adsorption energy of -1.64 eV, which is due to a strong interaction of H₂S with the Ni sites of the decorated surface. The PDOS plots also showed an overlap between the 3p and 3d orbitals of S and Ni atoms, respectively, which results from orbital hybridization during the formation of a covalent bond. Based on the results obtained in this study, it can be concluded that graphene sheet decorated with Ni atom has a great potential for the adsorption of H₂S molecules, and might be used for developing new gas sensors. Overall, the transition of the adsorption mechanism from physisorption to chemisorption was successfully captured by the model developed for use in future investigations.

Author Contributions: A.H.M. and S.H. designed the case study and carried out the computational calculations. Z.K. designed the figures and tables. A.S. analyzed and rechecked the results for correctness and wrote the original draft of the article. M.R.G., V.V., A.E. and M.R.S. analyzed the data and discussed the results. V.F. and A.C. reviewed and edited the article to give it its final form. All authors have read and agreed to the published version of the manuscript.

Funding: This research received no external funding.

Conflicts of Interest: The authors declare no conflict of interest.

References

1. Lins, V.F.C.; Guimaraes, E.M. Failure of a heat exchanger generated by an excess of SO₂ and H₂S in the Sulfur Recovery Unit of a petroleum refinery. *J. Loss Prev. Process Ind.* **2007**, *20*, 91–97. [[CrossRef](#)]
2. Mochizuki, Y.; Tsubouchi, N. Removal of Hydrogen Sulfide in Simulated Coke Oven Gas with Low-Grade Iron Ore. *Energy Fuels* **2017**, *31*, 8087–8094. [[CrossRef](#)]
3. Bak, C.-U.; Lim, C.-J.; Lee, J.-G.; Kim, Y.-D.; Kim, W.-S. Removal of sulfur compounds and siloxanes by physical and chemical sorption. *Sep. Purif. Technol.* **2019**, *209*, 542–549. [[CrossRef](#)]
4. Jiang, X.; Wu, J.; Jin, Z.; Yang, S.; Shen, L. Enhancing the removal of H₂S from biogas through refluxing of outlet gas in biological bubble-column. *Bioresour. Technol.* **2020**, *299*, 122621. [[CrossRef](#)]
5. Barbera, N.; Montana, A.; Indorato, F.; Arbouche, N.; Romano, G. Evaluation of the Role of Toxicological Data in Discriminating Between H₂S Femoral Blood Concentration Secondary to Lethal poisoning and Endogenous H₂S Putrefactive Production. *J. Forensic Sci.* **2017**, *62*, 392–394. [[CrossRef](#)]
6. Shefa, U.; Kim, M.-S.; Jeong, N.Y.; Jung, J. Antioxidant and Cell-Signaling Functions of Hydrogen Sulfide in the Central Nervous System. *Oxidative Med. Cell. Longev.* **2018**, *2018*, 17. [[CrossRef](#)] [[PubMed](#)]
7. Jia, X.; Zhang, H.; Zhang, Z.; An, L. First-principles investigation of vacancy-defected graphene and Mn-doped graphene towards adsorption of H₂S. *Superlattices Microstruct.* **2019**, *134*, 106235. [[CrossRef](#)]
8. Sudalma, S.; Purwanto, P.; Santoso, L.W. The Effect of SO₂ and NO₂ from Transportation and Stationary Emissions Sources to SO₄²⁻ and NO₃⁻ in Rain Water in Semarang. *Procedia Environ. Sci.* **2015**, *23*, 247–252. [[CrossRef](#)]
9. Santiago, R.; Lemus, J.; Outomuro, A.X.; Bedia, J.; Palomar, J. Assessment of ionic liquids as H₂S physical absorbents by thermodynamic and kinetic analysis based on process simulation. *Sep. Purif. Technol.* **2020**, *233*, 116050. [[CrossRef](#)]
10. Atlaskin, A.A.; Kryuchkov, S.S.; Yanbikov, N.R.; Smorodin, K.A.; Petukhov, A.N.; Trubyanov, M.M.; Vorotyntsev, V.M.; Vorotyntsev, I.V. Comprehensive experimental study of acid gases removal process by membrane-assisted gas absorption using imidazolium ionic liquids solutions absorbent. *Sep. Purif. Technol.* **2020**, *239*, 116578. [[CrossRef](#)]
11. Ge, K.; Wu, Y.; Wang, T.; Wu, J. Humidity swing adsorption of H₂S by fibrous polymeric ionic liquids (PILs). *Sep. Purif. Technol.* **2019**, *217*, 1–7. [[CrossRef](#)]

12. Zhang, H.-P.; Luo, X.-G.; Song, H.-T.; Lin, X.-Y.; Lu, X.; Tang, Y. DFT study of adsorption and dissociation behavior of H₂S on Fe-doped graphene. *Appl. Surf. Sci.* **2014**, *317*, 511–516. [[CrossRef](#)]
13. Alfonso, D.R. First-principles studies of H₂S adsorption and dissociation on metal surfaces. *Surf. Sci.* **2008**, *602*, 2758–2768. [[CrossRef](#)]
14. Zhang, M.; Fu, Z.; Yu, Y. Adsorption and decomposition of H₂S on the Ni(111) and Ni(211) surfaces: A first-principles density functional study. *Appl. Surf. Sci.* **2019**, *473*, 657–667. [[CrossRef](#)]
15. Sigot, L.; Ducom, G.; Germain, P. Adsorption of hydrogen sulfide (H₂S) on zeolite (Z): Retention mechanism. *Chem. Eng. J.* **2016**, *287*, 47–53. [[CrossRef](#)]
16. Berhe Gebreegziabher, T.; Wang, S.; Nam, H. Adsorption of H₂S, NH₃ and TMA from indoor air using porous corncob activated carbon: Isotherm and kinetics study. *J. Environ. Chem. Eng.* **2019**, *7*, 103234. [[CrossRef](#)]
17. Sitthikhankaew, R.; Predapitakkun, S.; Kiattikomol, R.; Pumhiran, S.; Assabumrungrat, S.; Laosiripojana, N. Comparative Study of Hydrogen Sulfide Adsorption by using Alkaline Impregnated Activated Carbons for Hot Fuel Gas Purification. *Energy Procedia* **2011**, *9*, 15–24. [[CrossRef](#)]
18. Zhang, X.; Cui, H.; Chen, D.; Dong, X.; Tang, J. Electronic structure and H₂S adsorption property of Pt₃ cluster decorated (8, 0) SWCNT. *Appl. Surf. Sci.* **2018**, *428*, 82–88. [[CrossRef](#)]
19. Srivastava, R.; Suman, H.; Shrivastava, S.; Srivastava, A. DFT analysis of pristine and functionalized zigzag CNT: A case of H₂S sensing. *Chem. Phys. Lett.* **2019**, *731*, 136575. [[CrossRef](#)]
20. Yousefian, Z.; Ghasemy, E.; Askarieh, M.; Rashidi, A. Theoretical studies on B, N, P, S, and Si doped fullerenes toward H₂S sensing and adsorption. *Phys. E Low-Dimens. Syst. Nanostruct.* **2019**, *114*, 113626. [[CrossRef](#)]
21. Faye, O.; Raj, A.; Mittal, V.; Beye, A.C. H₂S adsorption on graphene in the presence of sulfur: A density functional theory study. *Comput. Mater. Sci.* **2016**, *117*, 110–119. [[CrossRef](#)]
22. Rodriguez, J.A.; Maiti, A. Adsorption and Decomposition of H₂S on MgO(100), NiMgO(100), and ZnO(0001) Surfaces: A First-Principles Density Functional Study. *J. Phys. Chem. B* **2000**, *104*, 3630–3638. [[CrossRef](#)]
23. Ranea, V.A.; Dammig Quiña, P.L.; Yalet, N.M. General adsorption model for H₂S, H₂Se, H₂Te, NH₃, PH₃, AsH₃ and SbH₃ on the V₂O₅(001) surface including the van der Waals interaction. *Chem. Phys. Lett.* **2019**, *720*, 58–63. [[CrossRef](#)]
24. Bo, Z.; Guo, X.; Wei, X.; Yang, H.; Yan, J.; Cen, K. Density functional theory calculations of NO₂ and H₂S adsorption on the group 10 transition metal (Ni, Pd and Pt) decorated graphene. *Phys. E Low-Dimens. Syst. Nanostruct.* **2019**, *109*, 156–163. [[CrossRef](#)]
25. Faye, O.; Eduok, U.; Szpunar, J.; Samoura, A.; Beye, A. H₂S adsorption and dissociation on NH-decorated graphene: A first principles study. *Surf. Sci.* **2018**, *668*, 100–106. [[CrossRef](#)]
26. Ganji, M.D.; Sharifi, N.; Ardjmand, M.; Ahangari, M.G. Pt-decorated graphene as superior media for H₂S adsorption: A first-principles study. *Appl. Surf. Sci.* **2012**, *261*, 697–704. [[CrossRef](#)]
27. Cortés-Arriagada, D.; Villegas-Escobar, N.; Ortega, D.E. Fe-doped graphene nanosheet as an adsorption platform of harmful gas molecules (CO, CO₂, SO₂ and H₂S), and the co-adsorption in O₂ environments. *Appl. Surf. Sci.* **2018**, *427*, 227–236. [[CrossRef](#)]
28. Khodadadi, Z. Evaluation of H₂S sensing characteristics of metals-doped graphene and metals-decorated graphene: Insights from DFT study. *Phys. E Low-Dimens. Syst. Nanostruct.* **2018**, *99*, 261–268. [[CrossRef](#)]
29. Zhu, Y.; Murali, S.; Cai, W.; Li, X.; Suk, J.W.; Potts, J.R.; Ruoff, R.S. Graphene and Graphene Oxide: Synthesis, Properties, and Applications. *Adv. Mater.* **2010**, *22*, 3906–3924. [[CrossRef](#)]
30. Castro Neto, A.H.; Guinea, F.; Peres, N.M.R.; Novoselov, K.S.; Geim, A.K. The electronic properties of graphene. *Rev. Mod. Phys.* **2009**, *81*, 109–162. [[CrossRef](#)]
31. Lin, X.; Ni, J.; Fang, C. Adsorption capacity of H₂O, NH₃, CO, and NO₂ on the pristine graphene. *J. Appl. Phys.* **2013**, *113*, 034306. [[CrossRef](#)]
32. Gui, Y.; Hao, Z.; Li, X.; Tang, C.; Xu, L. Gas sensing of graphene and graphene oxide nanoplatelets to ClO₂ and its decomposed species. *Superlattices Microstruct.* **2019**, *135*, 106248. [[CrossRef](#)]
33. Shao, L.; Chen, G.; Ye, H.; Wu, Y.; Qiao, Z.; Zhu, Y.; Niu, H. Sulfur dioxide adsorbed on graphene and heteroatom-doped graphene: A first-principles study. *Eur. Phys. J. B* **2013**, *86*, 54. [[CrossRef](#)]
34. Ovsianytskyi, O.; Nam, Y.-S.; Tsybalenko, O.; Lan, P.-T.; Moon, M.-W.; Lee, K.-B. Highly sensitive chemiresistive H₂S gas sensor based on graphene decorated with Ag nanoparticles and charged impurities. *Sens. Actuators B Chem.* **2018**, *257*, 278–285. [[CrossRef](#)]
35. Song, Y.; Fang, W.; Hsu, A.L.; Kong, J. Iron (III) Chloride doping of CVD graphene. *Nanotechnology* **2014**, *25*, 395701. [[CrossRef](#)] [[PubMed](#)]

36. Gaboardi, M.; Bliersbach, A.; Bertoni, G.; Aramini, M.; Vlahopoulou, G.; Pontiroli, D.; Mauron, P.; Magnani, G.; Salviati, G.; Züttel, A.; et al. Decoration of graphene with nickel nanoparticles: Study of the interaction with hydrogen. *J. Mater. Chem. A* **2014**, *2*, 1039–1046. [[CrossRef](#)]
37. Hamed Mashhadzadeh, A.; Fathalian, M.; Ghorbanzadeh Ahangari, M.; Shahavi, M.H. DFT study of Ni, Cu, Cd and Ag heavy metal atom adsorption onto the surface of the zinc-oxide nanotube and zinc-oxide graphene-like structure. *Mater. Chem. Phys.* **2018**, *220*, 366–373. [[CrossRef](#)]
38. Mo, Y.; Li, H.; Zhou, K.; Ma, X.; Guo, Y.; Wang, S.; Li, L. Acetone adsorption to (BeO)₁₂, (MgO)₁₂ and (ZnO)₁₂ nanoparticles and their graphene composites: A density functional theory (DFT) study. *Appl. Surf. Sci.* **2019**, *469*, 962–973. [[CrossRef](#)]
39. Gui, Y.; Liu, D.; Li, X.; Tang, C.; Zhou, Q. DFT-based study on H₂S and SOF₂ adsorption on Si-MoS₂ monolayer. *Results Phys.* **2019**, *13*, 102225. [[CrossRef](#)]
40. Ganji, M.; Sharifi, N.; Ahangari, M.G. Adsorption of H₂S molecules on non-carbonic and decorated carbonic graphenes: A van der Waals density functional study. *Comput. Mater. Sci.* **2014**, *92*, 127–134. [[CrossRef](#)]
41. Zhang, Y.-H.; Yue, L.-J.; Gong, F.-L.; Li, F.; Zhang, H.-L.; Chen, J.-L. Highly enhanced H₂S gas sensing and magnetic performances of metal doped hexagonal ZnO monolayer. *Vacuum* **2017**, *141*, 109–115. [[CrossRef](#)]
42. Ordejón, P.; Artacho, E.; Soler, J.M. Self-consistent order- N density-functional calculations for very large systems. *Phys. Rev. B* **1996**, *53*, R10441–R10444. [[CrossRef](#)]
43. Soler, J.M.; Artacho, E.; Gale, J.D.; García, A.; Junquera, J.; Ordejón, P.; Sánchez-Portal, D. The SIESTA method for ab initio order- N materials simulation. *J. Phys. Condens. Matter* **2002**, *14*, 2745. [[CrossRef](#)]
44. Xu, W.; EA Kelly, R.; Otero, R.; Schöck, M.; Lægsgaard, E.; Stensgaard, I.; Kantorovich, L.N.; Besenbacher, F. Probing the Hierarchy of Thymine–Thymine Interactions in Self-Assembled Structures by Manipulation with Scanning Tunneling Microscopy. *Small* **2007**, *3*, 2011–2014. [[CrossRef](#)]
45. Junquera, J.; Paz, Ó.; Sánchez-Portal, D.; Artacho, E. Numerical atomic orbitals for linear-scaling calculations. *Phys. Rev. B* **2001**, *64*, 235111. [[CrossRef](#)]
46. Balabin, R.M. Enthalpy difference between conformations of normal alkanes: Intramolecular basis set superposition error (BSSE) in the case of n-butane and n-hexane. *J. Chem. Phys.* **2008**, *129*, 164101. [[CrossRef](#)]
47. Ghorbanzadeh Ahangari, M.; Fereidoon, A.; Hamed Mashhadzadeh, A. Interlayer interaction and mechanical properties in multi-layer graphene, Boron-Nitride, Aluminum-Nitride and Gallium-Nitride graphene-like structure: A quantum-mechanical DFT study. *Superlattices Microstruct.* **2017**. [[CrossRef](#)]
48. Ansari, R.; Mirnezhad, M.; Rouhi, H. A first principles study on the mechanical properties of hexagonal zinc oxide sheets. *Superlattices Microstruct.* **2015**, *79*, 15–20. [[CrossRef](#)]
49. Marana, N.L.; Casassa, S.; Longo, E.; Sambrano, J.R. Structural, Electronic, Vibrational, and Topological Analysis of Single-Walled Zinc Oxide Nanotubes. *J. Phys. Chem. C* **2016**, *120*, 6814–6823. [[CrossRef](#)]
50. Hamed Mashhadzadeh, A.; Ghorbanzadeh Ahangari, M.; Dadrasi, A.; Fathalian, M. Theoretical studies on the mechanical and electronic properties of 2D and 3D structures of Beryllium-Oxide graphene and graphene nanobud. *Appl. Surf. Sci.* **2019**, *476*, 36–48. [[CrossRef](#)]
51. Rastegar, S.F.; Ahmadi Peyghan, A.; Soleymannabadi, H. Ab initio studies of the interaction of formaldehyde with beryllium oxide nanotube. *Phys. E Low-Dimens. Syst. Nanostruct.* **2015**, *68*, 22–27. [[CrossRef](#)]
52. Ahangari, M.G.; Mashhadzadeh, A.H.; Fathalian, M.; Dadrasi, A.; Rostamiyan, Y.; Mallahi, A. Effect of various defects on mechanical and electronic properties of zinc-oxide graphene-like structure: A DFT study. *Vacuum* **2019**, *165*, 26–34. [[CrossRef](#)]
53. Rostamiyan, Y.; Mohammadi, V.; Hamed Mashhadzadeh, A. Mechanical, electronic and stability properties of multi-walled beryllium oxide nanotubes and nanopeapods: A density functional theory study. *J. Mol. Modeling* **2020**, *26*, 76. [[CrossRef](#)]
54. Pawar, V.; Jha, P.K.; Panda, S.K.; Jha, P.A.; Singh, P. Band-Gap Engineering in ZnO Thin Films: A Combined Experimental and Theoretical Study. *Phys. Rev. Appl.* **2018**, *9*, 054001. [[CrossRef](#)]
55. Arif, A.; Belahssen, O.; Gareh, S.; Benramache, S. The calculation of band gap energy in zinc oxide films. *J. Semicond.* **2015**, *36*, 013001. [[CrossRef](#)]
56. Baumeier, B.; Krüger, P.; Pollmann, J. Structural, elastic, and electronic properties of SiC, BN, and BeO nanotubes. *Phys. Rev. B* **2007**, *76*, 085407. [[CrossRef](#)]
57. Wu, W.; Lu, P.; Zhang, Z.; Guo, W. Electronic and Magnetic Properties and Structural Stability of BeO Sheet and Nanoribbons. *ACS Appl. Mater. Interfaces* **2011**, *3*, 4787–4795. [[CrossRef](#)]

58. Derakhshandeh, M.; Anaraki-Ardakani, H. A computational study on the experimentally observed sensitivity of Ga-doped ZnO nanocluster toward CO gas. *Phys. E Low-Dimens. Syst. Nanostruct.* **2016**, *84*, 298–302. [[CrossRef](#)]
59. Hamed Mashhadzadeh, A.; Fereidoon, A.; Ghorbanzadeh Ahangari, M. Combining density functional theory-finite element multi-scale method to predict mechanical properties of polypropylene/graphene nanocomposites: Experimental study. *Mater. Chem. Phys.* **2017**, *201*, 214–223. [[CrossRef](#)]
60. Hamed Mashhadzadeh, A.; Ghorbanzadeh Ahangari, M.; Salmankhani, A.; Fataliyan, M. Density functional theory study of adsorption properties of non-carbon, carbon and functionalized graphene surfaces towards the zinc and lead atoms. *Phys. E Low-Dimens. Syst. Nanostruct.* **2018**, *104*, 275–285. [[CrossRef](#)]
61. Ghorbanzadeh Ahangari, M.; Salmankhani, A.; Imani, A.H.; Shahab, N.; Hamed Mashhadzadeh, A. Density Functional Theory Study on the Mechanical Properties and Interlayer Interactions of Multi-layer Graphene: Carbonic, Silicon-Carbide and Silicene Graphene-like Structures. *Silicon* **2019**, *11*, 1235–1246. [[CrossRef](#)]
62. Ergun, S. Structure of Graphite. *Nat. Phys. Sci.* **1973**, *241*, 65–67. [[CrossRef](#)]
63. Mashhadzadeh, A.H.; Vahedi, A.M.; Ardjmand, M.; Ahangari, M.G. Investigation of heavy metal atoms adsorption onto graphene and graphdiyne surface: A density functional theory study. *Superlattices Microstruct.* **2016**, *100*, 1094–1102. [[CrossRef](#)]
64. Sharifi, N.; Falamaki, C.; Ahangari, M.G. DFT study of Au adsorption on pure and Pt-decorated γ -alumina (110) surface. *Appl. Surf. Sci.* **2017**, *416*, 390–396. [[CrossRef](#)]

Publisher's Note: MDPI stays neutral with regard to jurisdictional claims in published maps and institutional affiliations.



© 2020 by the authors. Licensee MDPI, Basel, Switzerland. This article is an open access article distributed under the terms and conditions of the Creative Commons Attribution (CC BY) license (<http://creativecommons.org/licenses/by/4.0/>).